Journal of Catalysis 271 (2010) 401–412

Contents lists available at ScienceDirect

Journal of Catalysis

journal homepage: www.elsevier.com/locate/jcat

Deactivation of PtH-MFI bifunctional catalysts by coke formation during benzene alkylation with ethane

Li Min Chua, Tanya Vazhnova, Timothy J. Mays, Dmitry B. Lukyanov, Sean P. Rigby *

Department of Chemical Engineering, University of Bath, Claverton Down, Bath BA2 7AY, UK

ARTICLE INFO

Article history:
Received 21 October 2009
Revised 22 February 2010
Accepted 24 February 2010
Available online 2 April 2010

Keywords:
Zeolite
Deactivation
Coking
Percolation theory
Gas sorption
Mass transport

ABSTRACT

The alkylation reaction of benzene with ethane was studied at 370 °C over two Pt-containing MFI catalysts with Si/Al ratios of 15 and 40. The deactivation of the PtH-MFI-15 catalyst was found to be more significant, when compared with the PtH-MFI-40 catalyst, as a result of differences between the two catalysts in the formation of coke. The differing locations of the coke deposition were found to profoundly affect the product selectivity and deactivation behaviour of the two PtH-MFI catalysts. Results from gas sorption and X-ray diffraction experiments showed that coke is preferentially formed towards the centre of crystallites of the PtH-MFI-15 catalyst, as opposed to coke deposition on the outside surface of the PtH-MFI-40 crystallites, subsequently blocking entrance to the zeolite channels. Partial blockage of the internal pore structure of the PtH-MFI-15 catalyst with coke decreased the diffusion length within the PtH-MFI-15 crystallites. The effect of this reduction in the diffusion length within the PtH-MFI-15 crystallites is consistent with the observed decreasing *para*-selectivity of the diethylbenzene (DEB) isomers with time-on-stream. These findings are in contrast to the typical effect of coking, where, generally, the selectivity of *para*- isomers would be enhanced with coke deposition.

1. Introduction

Ethylbenzene is an important intermediate in the production of polystyrene. The worldwide capacity for ethylbenzene production was estimated to be 23 million tonnes per year in 2001, with a projected annual growth rate of approximately 4% [1]. Benzene alkylation with ethene is a vital step in the synthesis of ethylbenzene. However, the use of ethene is not favourable as it is the product of highly energy intensive processes, such as ethane and naphtha reforming [2]. Due to environmental and economical concerns, ethane can be used as an alternative alkylating agent.

Recently, a new bifunctional PtH-ZSM-5 zeolite catalyst has been studied for benzene alkylation with ethane:

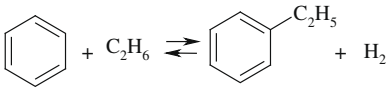

(1)

where the optimum reaction temperature (370 °C) [3] and the analysis of the kinetics of the alkylation reaction have been discussed previously [4]. The ZSM-5 type zeolite was chosen because it has become a well-known solid catalyst for acid-catalysed reactions due to its shape-selectivity property [5] and its high resistance to deactivation in comparison with other commercial zeolite catalysts [6]. Despite the promising results demonstrated by the PtH-ZSM-5 catalysts for the benzene alkylation reaction [3,4], the deactivation of the catalyst, caused by deposition of carbonaceous compounds, potentially could limit the development of this process. However, the details of the mechanism of coke formation during the ethylbenzene production process have remained unknown until now.

Catalyst deactivation, as a result of coke formation, has been a challenge in the catalyst industry for many hydrocarbon processes. Extensive studies on the subject of coke and catalyst deactivation have been previously carried out on other hydrocarbon-processing reactions [5–8], though not for the reaction of benzene alkylation with ethane. Two mechanisms of coking have been identified: pore blocking where coke blocks the access of reactants to active sites and active site coverage where coke poisons the active sites responsible for the reaction [6,7]. Depending on the loss of adsorption capacity of the coked catalyst and the amount of coke formed, Bibby et al. [5] and Guisnet and Magnoux [8] were able to identify the different modes of deactivation and the broad location of the coke deposition. This method was then employed by other researchers [6,7,9] to further understand the effect of coke formation in different catalytic reactions.

Modification of the ZSM-5 catalysts, by chemical treatment with different agents, or by varying the crystallite size of the catalyst, or by coking, have been reported to influence the product distribution of shape-selective reactions [6,10,11]. The effect of coke

* Corresponding author.
E-mail address: S.P.Rigby@bath.ac.uk (S.P. Rigby).

0021-9517/$ - see front matter © 2010 Elsevier Inc. All rights reserved.
doi:10.1016/j.jcat.2010.02.029

deposition on *para*-selectivity was found to be dependent on the location of coke, specifically whether it was located either within the internal pore structure or on the external surface of the zeolite catalyst [6,11]. For example, some partially deactivated catalysts have been shown to become less *para*-selective because of coke deposition by pore filling, as demonstrated by Soleto et al. [6], who studied the deactivation of the toluene alkylation with methanol reaction on ZSM-5 catalysts. Conversely, Chen et al. [11] showed that, with increasing coke content, *para*-diethylbenzene (DEB) selectivity increased during the disproportionation of ethylbenzene (EB). Similarly, Lin et al. [12] showed that pore blockage, as a result of coke formation, caused an increase in the *para*-xylene selectivity with prolonged time-on-stream (TOS). However, this previous work on the influence of coking on selectivity has only considered gross features of the spatial distribution of coke laydown on selectivity, such as the balance between external (pore mouth blocking) and internal laydown. Internal coke laydown can affect intrinsic diffusivity (through impact on pore connectivity) and/or diffusional path length. Hence, gross characteristics are insufficient to fully understand the impact of coking on mass transfer, and subsequently selectivity.

In this work, a more detailed study will be made of the particular spatial distribution of coke laydown. A detailed analysis of structural characterisation data using percolation concepts, combined with reaction and transport experimental data, allows a more definitive description of the coking behaviour to be obtained than previously. It will be shown that these studies allow greater insight into the deactivation mechanism during the benzene alkylation reaction with ethane over PtH-MFI catalysts.

A series of bifunctional Pt-H-MFI catalysts, with Si/Al ratios of 15 and 40, coked to different extents were studied to investigate relationships between the evolution of the pore structure of the zeolite catalysts and its effect on adsorption kinetics, transport properties, and changes to the product distribution from the benzene alkylation reaction. A diverse combination of analytical techniques, including thermogravimetric analysis (TGA), X-ray diffraction (XRD), scanning electron microscopy (SEM) and gas sorption measurements were employed in this work to understand the phenomena related to coking.

2. Experimental section

2.1. Catalyst preparation

Two H-MFI (ZSM-5) zeolites with a Si/Al ratio of 15 and 40 (ZEOLYST) were used as the parent catalysts for the benzene alkylation reaction. The Pt-containing zeolite catalysts, defined as PtH-MFI-15 and PtH-MFI-40, were prepared by incipient wetness impregnation of parent H-MFI (Si/Al of 15 and 40), using an aqueous solution of tetraamine–platinum (II) nitrate, $Pt(NH_3)_4(NO_3)_2$. The catalysts were prepared such that the ultimate platinum content for both was 1 wt%. After impregnation, the catalysts were dried at room temperature and then calcined in a muffle furnace at 530 °C for 4 h at a heating rate of 1 °C min^{-1}. For the reaction studies, the prepared bifunctional catalysts were pressed into discs and then crushed and sieved to obtain particle sizes in the range of 250–710 μm.

2.2. Kinetic studies

Benzene alkylation with ethane was carried out at atmospheric pressure in a continuous flow reactor at 370 °C with 9:1 molar feed ratio of ethane to benzene. The catalyst loading of 500 mg was activated by heating in air at 530 °C for 4 h, and then reduced in hydrogen at 500 °C for 1 h. After being run for different times-on-stream (TOS), the reactor was purged with nitrogen (30 ml min^{-1}) for 0.5 h at the reaction temperature and then cooled down to room temperature in a nitrogen atmosphere. The catalysts were then unloaded from the reactor for further analyses.

The conversion of benzene and ethane and the selectivity of products produced from benzene at a certain TOS were defined as follows. The conversion X_i of reactant i was defined as:

$$Conversion,\ X_i = \frac{C_{i0} - C_i}{C_{i0}} \times 100\%, \tag{2}$$

whereas the selectivity, S_i, of product i formed from benzene was defined as:

$$Selectivity,\ S_i = \frac{C_i}{C_{B0} - C_B} \times 100\%, \tag{3}$$

where C_{i0} is the initial concentration of species i, C_i is the concentration of species i in the reaction mixture, C_{B0} is the initial concentration of benzene, and C_B is the concentration of benzene in the reaction mixture.

2.3. Catalyst characterisation

2.3.1. Themogravimetric analysis (TGA)

Thermogravimetric analysis of the coke content of the discharged PtH-MFI catalysts was performed in a Setaram TGA92 thermogravimetric analyzer. Coked samples were heated from room temperature to 1000 °C at a rate of 10 °C min^{-1} in flowing, dry air.

2.3.2. Gas sorption

The structural characteristics of the PtH-MFI samples were determined by gas sorption. Nitrogen and argon sorption experiments were each carried out using a Micromeritics ASAP 2020 volumetric apparatus at 77 K. Ethane sorption experiments were performed on a Hiden IGA at a range of temperatures between 10 and 30 °C. Prior to adsorption analysis, the samples were heated under vacuum at 250 °C, until no further mass loss is observed, to remove any physisorbed water. The temperature of the thermal pre-treatment was chosen to avoid the removal of coke deposited during the preparation process.

2.3.3. X-ray diffraction (XRD)

Powder X-ray diffraction experiments were carried out using a D8 Advance Bruker X-ray diffractometer. Diffraction patterns were recorded using Cu Kα radiation at 40 kV, 30 mA, and a scan rate of 1° min^{-1}.

2.3.4. Scanning electron microscopy (SEM)

Scanning electron microscopy experiments were conducted on a JEOL JSM6480LV system operating at 15 kV. The samples were coated with a thin carbon layer before imaging analyses were carried out. The effect of coke deposition on the platinum particles impregnated onto the H-MFI catalysts was studied by backscattered electron imaging.

3. Percolation modelling

The model of the ZSM-5 lattice used is adapted from previous work by Trout et al. [13] and is presented in Fig. 1. The black dots represent the adsorption sites in the intersections (sites) while the grey dots represent the straight/zig-zag channels (bonds). There are 12 lattice points per unit cell; four in the intersections (there being four intersections in the unit cell) and eight in the straight and zig-zag channels. A large lattice size was used to represent a large zeolite crystallite to avoid finite size effects on the percola-

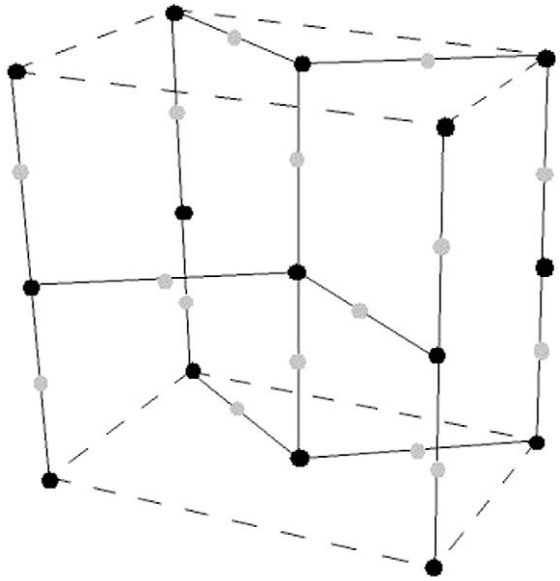

Fig. 1. Lattice model of ZSM-5 (adapted from [13]) black dots represent the adsorption sites in the intersections (sites) while the grey dots represent the straight/zig-zag channels (bonds).

tion accessibility function. It was found that by increasing the lattice size above 48 × 48 × 48, the accessibility function did not then change with lattice size. The simulation work in this study was carried out on a 96 × 96 × 96 lattice with 13,824 unit cells, giving a total of 165,888 accessible lattice points.

A potential model for homogeneous deactivation of a typical zeolite crystallite involves the blocking of the bonds and intersections of the lattice generated. In this study, bond-site percolation was investigated for the ZSM-5 lattice. The intersections and bonds that were blocked were chosen at random according to a probability weighted by their volume in the real zeolite. The coke molecules could only occupy the bonds and intersections if they were previously empty. Once a bond or intersection was occupied by coke, no further occupancy was allowed.

For calculations of accessibility, a layer of diffusing molecules was placed along the boundaries of the lattice to represent the nitrogen (or argon) bulk phase during adsorption. These molecules then penetrated into the pore network to identify accessible bonds and sites. Any pores plugged with coke were considered inaccessible and potentially barred the way for further penetration. If pores were unplugged, or not blocked by coke molecules, but were completely surrounded by blocked pores, these isolated clusters were also considered as not accessible. Simulations were repeated for sets of new lattices, and random number seeds, and average values for the accessibility fraction were taken, in order to obtain a typical result for random dispersion/distribution of coke molecules in the lattice/crystallites.

4. Results

4.1. Alkylation of benzene with ethane

4.1.1. Effect of time-on-stream (TOS) on benzene and ethane conversion

The alkylation reaction of benzene with ethane was carried out on Pt-supported H-MFI catalysts of Si/Al ratio of either 15 or 40 with a contact time of 0.32 h. Fig. 2A and B demonstrate the performance of the two bifunctional zeolite catalysts used in this work for benzene alkylation with ethane. The activity of the PtH-MFI-15 catalyst decreased with TOS, as shown by the decreasing ben-

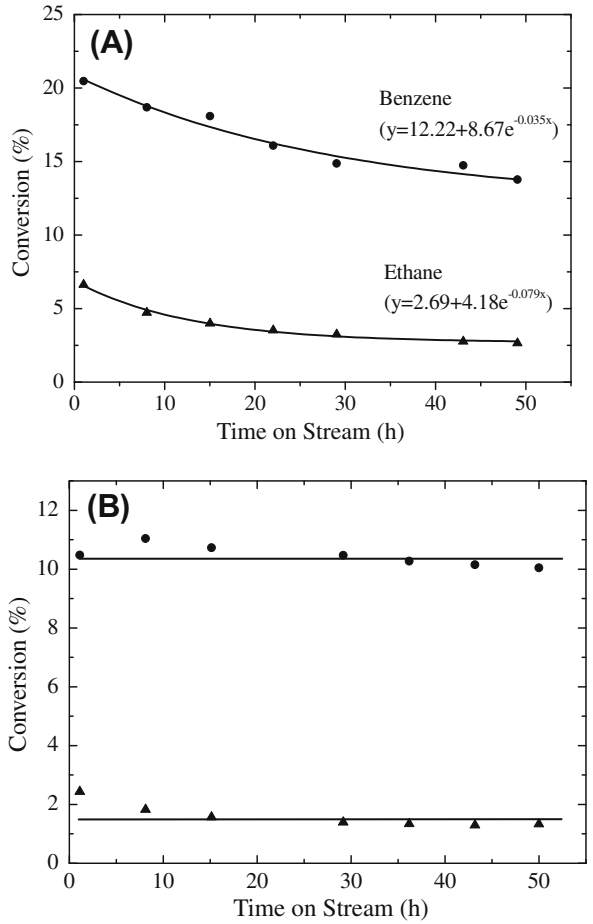

Fig. 2. Effect of time-on-stream (TOS) on (●) benzene and (▲) ethane conversions over PtH-MFI-15 (A) and PtH-MFI-40 (B) catalysts at 370 °C. Curves in (A), and the equations, represent least squares best fits using a shifted exponential decay model (y is conversion, x is TOS). Lines in (B) represent best fits assuming constant conversion.

zene and ethane conversion with TOS (Fig. 2A). The conversion of ethane decreased more rapidly compared to the drop in benzene conversion during the 48 h on-stream as demonstrated by the fitted exponential decay time constants of 0.079 ± 0.009 h^{-1} for ethane and 0.035 ± 0.014 h^{-1} for benzene.

In contrast to the behaviour of the PtH-MFI-15 catalyst, no significant changes were observed in benzene and ethane conversion after 48 h on-stream for the PtH-MFI-40 catalyst (Fig. 2B). The catalyst's activity remained stable for the reaction time tested.

4.1.2. Variation of the product selectivities with time-on-stream (TOS)

In addition to the ethane dehydrogenation reaction and benzene alkylation with ethene into ethylbenzene (EB), the presence of alkenes in the reaction mixture leads to a number of side reactions. Three categories of side reactions were identified during the benzene alkylation with ethane reaction, namely hydrogenolysis of ethane, alkene oligomerization and cracking reactions, and transformation of EB reactions [3].

While the conversion of the reactants decreased (PtH-MFI-15) or remained constant (PtH-MFI-40), the selectivity of the desired product, EB, was increasing with TOS (Fig. 3). Further alkylation of EB with ethene produces diethylbenzene (DEB). All three isomers of DEB (*para*-, *meta*- and *ortho*-) were observed in the products produced over the PtH-MFI-40 catalyst (Fig. 4B). However, *ortho*-DEB was not observed for the reaction carried out with the PtH-MFI-15 catalyst (Fig. 4A). The selectivity to *meta*-DEB

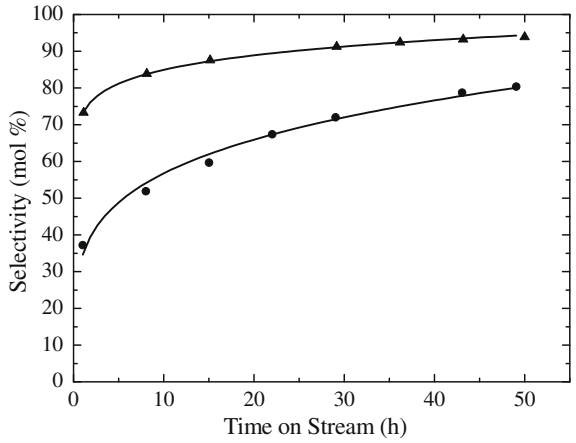

Fig. 3. Effect of time-on-stream (TOS) on EB selectivity in aromatic products for PtH-MFI-15 (●) and PtH-MFI-40 (▲) catalysts. The lines shown are to guide the eye.

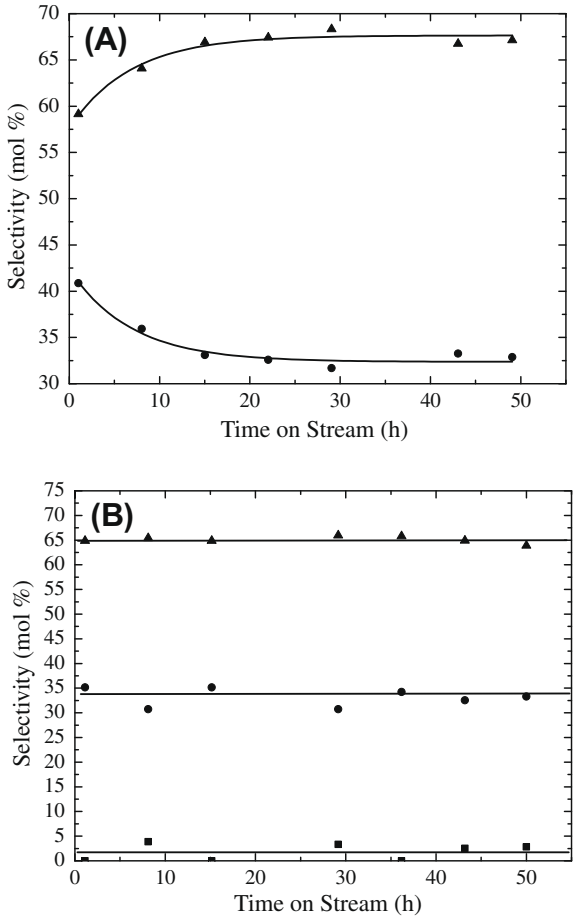

Fig. 4. Variation of *meta*-DEB (▲), *para*-DEB (●) and *ortho*-DEB (■) isomer selectivities with time-on-stream (TOS) over PtH-MFI-15 (A) and PtH-MFI-40 (B) catalysts. The lines shown are to guide the eye.

increased, while the *para*-DEB selectivity decreased, for the PtH-MFI-15 catalyst which deactivated with time. No significant changes were observed in the selectivities of all DEB isomers during the course of the reaction with PtH-MFI-40 catalyst. The ratio of *meta*-DEB to *para*-DEB expected at thermodynamic equilibrium at 370 °C is 1.81.

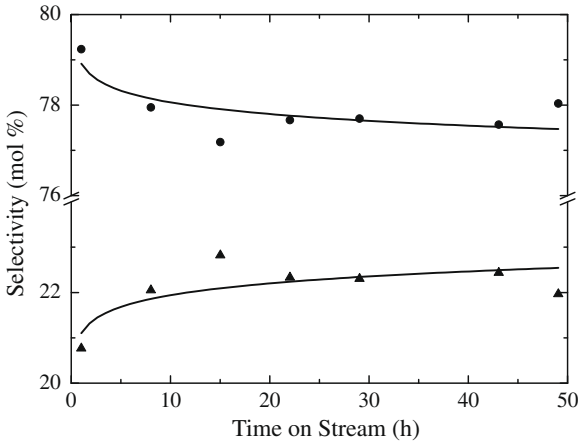

Fig. 5. Variation of *meta*- + *para*-xylenes (●) and *ortho*-xylene (▲) isomer selectivity with time-on-stream (TOS) over PtH-MFI-15 catalyst. The solid lines shown are to guide the eye.

The formation of xylenes observed in the product stream can be a result of the hydroisomerization reaction of EB, as suggested by Moreau et al. [14]. Fig. 5 shows an increasing selectivity towards the *ortho*-xylene isomer, while the *para*- + *meta*-xylene selectivity decreased, with TOS, when the reaction was carried out over the PtH-MFI-15 catalyst. Separate linear regression fits to each of the data sets shown in Fig. 5 give rise to two straight lines with non-zero gradients but with opposite signs and where, for both, the standard error range does not include zero, thereby suggesting the observed opposite trends in selectivity are real. The ratio of *para*- + *meta*-xylene to *ortho*-xylene expected at thermodynamic equilibrium at 370 °C is 3.24.

Further side products were also present. The alkylation reaction of benzene with propene (the product of alkene oligomerization and cracking) into isopropylbenzene was a major competing reaction to the main EB formation reaction. Another side product, which was present in a large quantity, was toluene (together with methane), which was formed via the EB hydrogenolysis reaction. Subsequently, toluene reacts with ethene, via an alkylation reaction, to produce ethyltoluene which had a high selectivity in the aromatic product stream.

4.2. Nature of coke

FT-IR spectroscopy has been widely used to study the chemical nature of coke deposits. IR spectra (not shown here) were obtained for the samples studied here, and will be presented in a future publication, where the acidity–activity correlation will be the main topic of discussion. Only details specifically relevant to the present study will be discussed here. An IR band at 1600 cm^{-1}, known as the 'coke band', was clearly seen for the PtH-MFI-15 sample after 48 h on-stream, indicating the presence of polyaromatic species. A doublet at 1369 and 1382 cm^{-1}, which is typical of branched alkanes, was also observed, suggesting that the coke deposits have some paraffinic character (e.g. alkyl chains attached to polyaromatics).

The FT-IR spectra obtained are similar to the results obtained by Uguina et al. [9] for a ZSM-5 sample coked with toluene. In addition, the chemical character of the coke deposits is consistent with the results reported for the alkylation reaction of toluene with methanol by Sotelo et al. [6]. Given the similarities between the FT-IR spectra obtained and the ones reported previously, the nature of the coke deposit was assumed to be the same. Hence, coke of density in the range between 1.2 g cm^{-3} and 1.3 g cm^{-3} [6,7,9] was assumed.

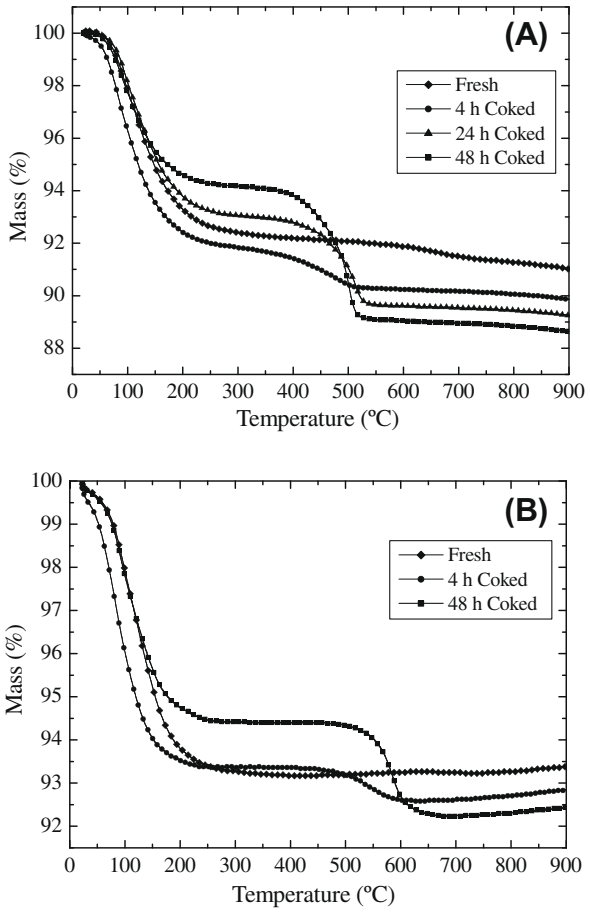

Fig. 6. Thermogravimetric profiles for fresh and coked PtH-MFI-15 (A) and PtH-MFI-40 (B) catalysts.

4.3. TGA/coke content measurements

The mass percentages of the coke deposits on the spent PtH-MFI catalysts were determined via thermogravimetric analysis. Coke densities of 1.2 g cm^{-3} and 1.3 g cm^{-3} [6,7] were then used to calculate the coke volume (V_c). The uncertainties in the coke densities at each TOS were taken into account when evaluating the standard errors in coke volume (V_c) and fraction of unplugged pores, f.

Fig. 6 shows the change in mass of the catalysts with temperature. Two distinct mass loss steps were observed for coked catalysts. The mass loss between room temperature and 300 °C was attributed to desorption of water, while the second step, between temperatures of 300 °C and 900 °C, was a result of oxidation of the carbonaceous deposits arising from the alkylation reaction.

The amount of coke content, expressed as a ratio to the fresh catalyst mass, was calculated as follows:

$$\textit{Coke Content}\ (\textit{mass}\%) = \frac{w_{300} - w_{900}}{w_{900}} \times 100\% \qquad (4)$$

where w_T is the mass of the sample at temperature T.

The amount of coke formed on the used catalysts at different TOS is summarised in Table 1. In spite of an increase in the coke content, the rate of coke deposition declined with time after a rapid increase in the amount of carbonaceous deposits at 4 h TOS.

The main steps in the TGA curves for the coked samples differ in their positions and intensities when compared with the fresh catalyst. The observed shift in the second step to higher temperature with TOS (particularly comparing 4 h and 48 h TOS) could be an indication of the presence of more heavy species/aromatics in the coked catalysts, or that the coke being oxidised was then in regions which were more inaccessible, and therefore required higher temperature for removal from the catalyst bed. It is also possible that the shifts in TGA steps to higher temperatures indicate a higher degree of structural order in the deposited cokes, and hence lower oxidation reactivity.

Table 1
Values of coke content on coked PtH-MFI catalysts after different time-on-stream (TOS). The coke content measured has a standard error of ±0.03%.

Time-on-stream (h)	Total coke (mass %)	
	PtH-MFI-15	PtH-MFI-40
4	1.83	0.76
24	3.39	–
48	5.61	2.00

4.4. Effect of coke on adsorption capacity of nitrogen, argon and ethane

In order to understand the influence of coking on the pore structure of PtH-MFI catalysts, the discharged catalysts were examined by adsorption studies with different adsorptives. Since nitrogen possesses a significant, permanent quadrupole moment, which can specifically interact with certain surface sites, argon isotherms were also obtained for comparison purposes. Ethane adsorption isotherms were also obtained since ethane is a key participant in the reactions.

4.4.1. Nitrogen and argon adsorption

The nitrogen and argon adsorption isotherms for fresh and deactivated PtH-MFI catalysts are shown in Figs. 7 and 8. The reproducibility of the isotherms was confirmed by comparing with duplicate isotherms also obtained. The effect of pre-treatment duration was also investigated and it was confirmed that the architecture of the catalyst was not influenced by the pre-treatment conditions. All uptake values for the isotherms for coked samples were renormalized for the coke content (using the TGA data) and were thus expressed as the amount of gas adsorbed *per* unit mass of zeolite catalyst.

Adsorption isotherms for nitrogen and argon on PtH-MFI-15 catalysts showed a progressive decline in the total amount of argon and nitrogen adsorbed with TOS. Comparing the isotherms for the fresh and coked PtH-MFI-15 samples, it was observed that the uptake of nitrogen and argon was very large at low relative pressure and that the initial part of the isotherm was shifted to lower relative pressures for coked samples. The same trend was also observed on the PtH-MFI-40 catalysts, where the adsorption capacity of argon and nitrogen decreased with TOS.

The reversible regions of the experimental adsorption isotherms were fitted to a two-component model, comprising of Langmuir and BET components, to distinguish between the adsorption in the dual pore system of the zeolite catalyst. Since the PtH-MFI catalysts are made up of micropores within the zeolite crystallites and mesopores surrounding the zeolite crystallites, the Langmuir (Type I) model was used to represent adsorption within the microporous region, while a BET (Type II) model was used for adsorption in the pores outside of the zeolite crystallites. The ratios of the respective fitted adsorption capacity parameters to the total values for the fresh catalyst for both components were determined. From Table 2, it can be seen that the ratio of the BET component adsorption capacity parameter showed little change with TOS, relative to the Langmuir component, for the PtH-MFI-15 catalysts. In contrast, for the PtH-MFI-40 catalyst, there was a much more significant drop, proportionately, in the adsorption capacity ratio for

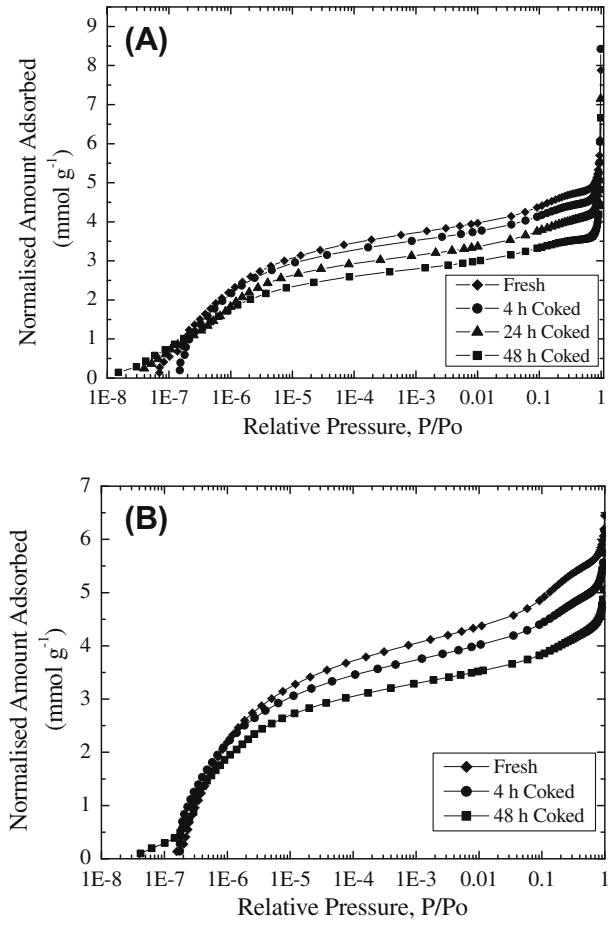

Fig. 7. Nitrogen adsorption isotherms at 77 K for PtH-MFI-15 (A) and PtH-MFI-40 (B) catalysts. (The lines shown for coked samples are to guide the eye.)

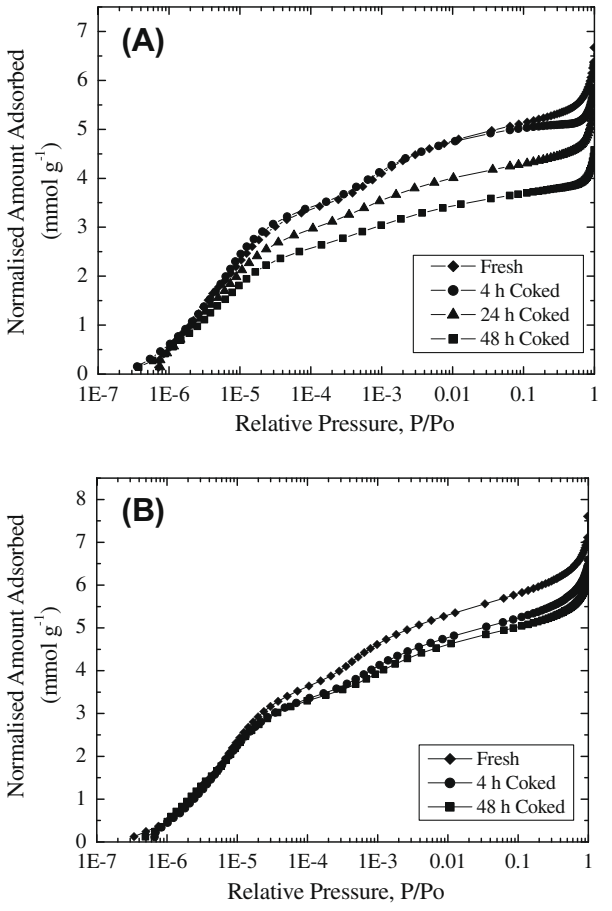

Fig. 8. Argon adsorption isotherms at 77 K for PtH-MFI-15 (A) and PtH-MFI-40 (B) catalysts. (The lines shown for coked samples are to guide the eye.)

the BET component with TOS when compared to the Langmuir component.

The external accessibility of the microporosity of the coked PtH-MFI catalysts was investigated based on the pore volumes determined from the experimental adsorption isotherms after subtracting the volumes occupied by coke molecules in the intercrystalline (mesopore) regions. The relationship between the accessible fraction of the unplugged pores (F) and total fraction of unplugged pores (f) is shown in Fig. 9. The values of F and f are determined by the following equations:

$$F = \frac{V(t = \mathrm{TOS})}{V(t = 0)} \tag{5}$$

where F is the accessibility fraction, $V(t = 0)$ is the pore volume for the fresh catalyst, and $V(t = \mathrm{TOS})$ corresponds to the externally accessible pore volume of the coked catalyst at different times-on-stream (TOS). The total fraction of unplugged pores, f, is given by:

$$f = \frac{V(t = 0) - V_c(t = \mathrm{TOS})}{V(t = 0)} \tag{6}$$

where $V_c(t = \mathrm{TOS})$ is the volume of coke at different TOS (t).

In the case of the PtH-MFI-15 catalysts at different TOS, the experimentally measured accessibility of the micropore lattice to nitrogen and argon still remained high even when the value of f corresponding to the percolation threshold of the MFI lattice, for the homogeneous reference case assuming randomly-distributed deposition of coke, is reached. This indicated that even with increasing coke deposition, all of the unblocked pores are still in the percolating cluster of the ZSM-5 network. The results thus showed that the potential scenario of homogeneous, random deposition of coke in the MFI crystallites during the alkylation reaction is incorrect.

4.4.2. Ethane adsorption

The effect of coke deposition on the adsorption of the key reactant, ethane was also studied and is presented in Fig. 10. The total

Table 2
Results of Langmuir and BET composite model fit to nitrogen (A) and argon (B) adsorption isotherms for PtH-MFI-15 and PtH-MFI-40 catalysts.

Time-on-stream (h)	W/W_o (Langmuir)		W/W_o (BET)	
	PtH-MFI-15	PtH-MFI-40	PtH-MFI-15	PtH-MFI-40
A. Nitrogen				
0	0.79 ± 0.05	0.75 ± 0.02	0.21 ± 0.02	0.25 ± 0.01
4	0.71 ± 0.05	0.67 ± 0.01	0.21 ± 0.02	0.22 ± 0.01
24	0.66 ± 0.05	–	0.21 ± 0.02	–
48	0.56 ± 0.04	0.67 ± 0.01	0.19 ± 0.02	0.19 ± 0.01
B. Argon				
0	0.76 ± 0.02	0.68 ± 0.01	0.24 ± 0.01	0.32 ± 0.01
4	0.74 ± 0.02	0.64 ± 0.01	0.25 ± 0.01	0.25 ± 0.01
24	0.61 ± 0.01	–	0.23 ± 0.01	–
48	0.55 ± 0.01	0.63 ± 0.01	0.20 ± 0.01	0.23 ± 0.01

Notes: W/W_o is the ratio of the adsorption capacity parameter of the relevant component, W, for the coked sample, to the corresponding total value, W_o, for the fresh catalyst.

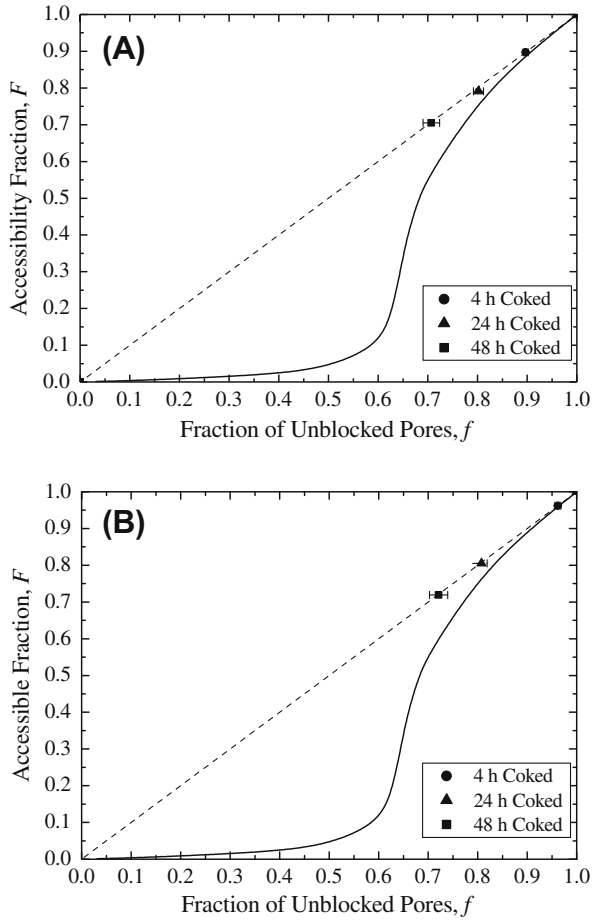

Fig. 9. Accessibility plot for nitrogen (A) and argon (B) – no percolation (dash line), Accessibility in a ZSM-5 lattice assuming random deposition of coke (solid line).

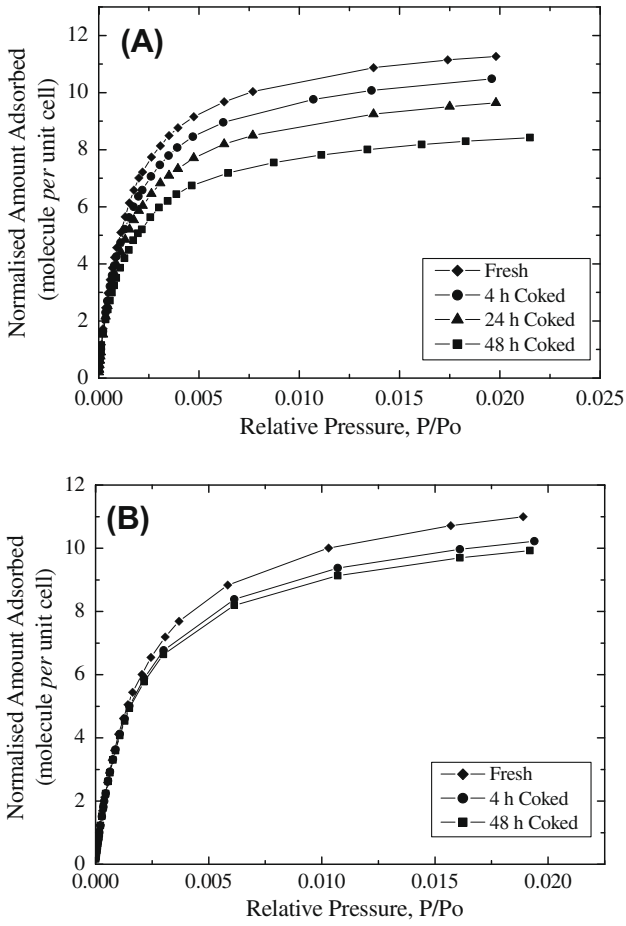

Fig. 10. Ethane adsorption isotherms for PtH-MFI-15 (A) and PtH-MFI-40 (B) catalysts at 30 °C. (The lines shown for coked samples are to guide the eye.)

amount of ethane adsorbed was corrected for the amount of coke formed, as described for nitrogen and argon adsorption. As with the nitrogen and argon adsorption results, the coke formed during the alkylation reaction caused a decrease in the adsorption capacity of the bifunctional PtH-MFI catalysts to ethane. The adsorption capacity of ethane is expressed in terms of molecules of ethane adsorbed *per* unit cell of the zeolite catalyst. This is instead of the mass of ethane adsorbed *per* unit mass of the zeolite catalyst which gives a less helpful understanding of the adsorption process.

At saturation, the total amount of ethane adsorbed for the fresh PtH-MFI-15 sample is 12 molecules *per* unit cell based on a mean obtained from three different adsorption temperatures. This value corresponds to the theoretical value of 12.6 molecules of ethane *per* unit cell calculated based upon adsorption of one molecule *per* each intersection in the unit cell at 16 °C [15]. When the coke content increased to 5.61 mass %, the saturation amount of ethane adsorbed for the PtH-MFI-15 catalyst decreased to eight molecules *per* unit cell.

4.5. X-ray diffraction

Fig. 11 shows the XRD patterns obtained for PtH-MFI-15 and PtH-MFI-40 catalysts at different TOS. The characteristic band at $2\theta = 22–25°$ was the main difference between the diffraction patterns of the coked catalysts and the fresh ones, so the spectra in these regions are expanded for clarity in Fig. 11. The changes in the relative intensities and diffraction peak positions were compared for the fresh and deactivated samples. For PtH-MFI-15 catalysts, with increasing TOS, the doublet nature of the peak at about 23–23.2° collapsed onto one peak at $2\theta = 23.12°$ with increasing intensity. The changes observed for the PtH-MFI-15 catalyst are believed to be related to the distortion of the zeolite lattice caused by deposition of coke within the lattice as reported in previous investigations [5,12,16].

In contrast to the behaviour of the PtH-MFI-15 catalyst, the position and the nature of the doublet peak was retained for the PtH-MFI-40 (Fig. 11B) catalyst even as the amount of coke formed increased with TOS.

4.6. Scanning electron microscopy

Typical examples of the backscattered scanning electron microscopy images of PtH-MFI catalysts at different TOS are shown in Fig. 12. In the backscattered images, the bright white dots represent the platinum particles on the surface of the zeolite crystallites. From, typically, images of three or more different, but identically sized, regions of the zeolite surface for each sample at different TOS, the number of platinum particles on the surface of the crystallites was calculated. These data are given in Table 3. The sampling errors in the surface platinum concentrations are given by the errors indicated in Table 3.

Fig. 12B clearly reveals more Pt particles on the surface of the PtH-MFI-40 catalyst than on the PtH-MFI-15 surface. The average concentration of platinum on the surface of PtH-MFI-15 crystallites remained the same before and after coking (Table 3). If coke were formed on the surface of the zeolite crystallites, it ought to obscure

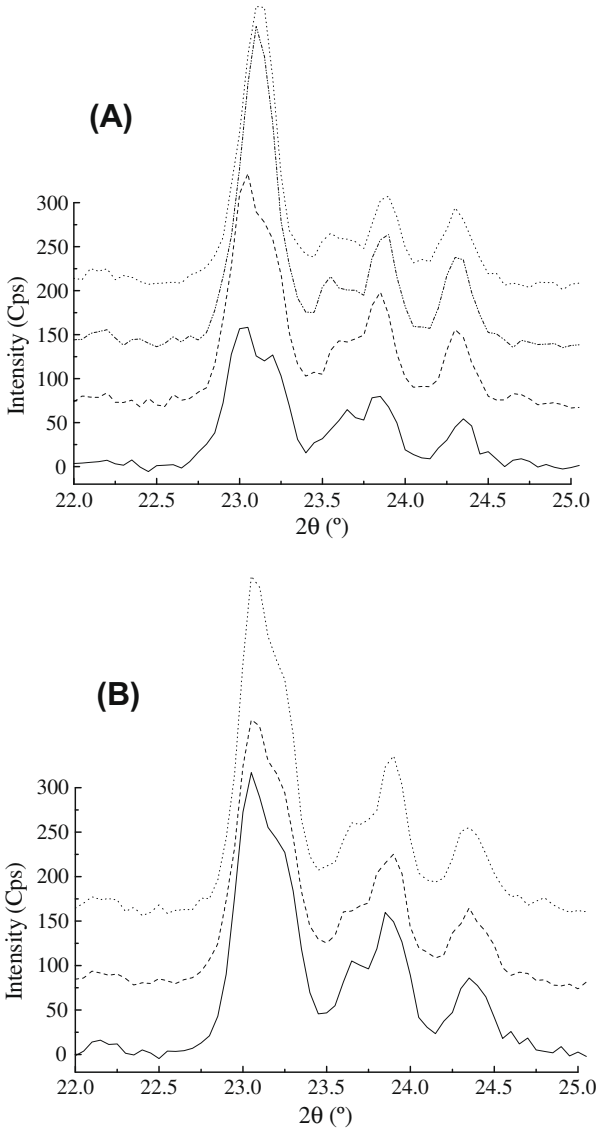

Fig. 11. XRD data for PtH-MFI-15 (A) and PtH-MFI-40 (B) catalysts: fresh (solid line), coked samples after 4 h (dashed line), 24 h (dash-dot-dot line) and 48 h (dotted line) on-stream.

at least some Pt particles, but this was not observed. Therefore, it can be assumed that coke was deposited inside the crystallites of the PtH-MFI-15 catalyst, supporting the diffraction results discussed above. The reduction in the Pt concentration with TOS (Table 3) suggests the deposition of coke on the surface of the PtH-MFI-40 crystallites.

4.7. Isosteric heat of adsorption, Q_{st}

The Q_{st} of ethane was determined from the series of adsorption isotherms obtained at three different temperatures. The isosteric method is based on the Clausius–Clapeyron equation:

$$\Delta H_{T,\Gamma} = R\left(\frac{\partial(\mathrm{In}[p])}{\partial(1/T)}\right)_{\Gamma} \tag{7}$$

where ΔH is the differential molar enthalpy of adsorption (kJ mol^{-1}) at constant amount adsorbed, Γ (mg mg^{-1}) (Q_{st}), at temperature T (K), R is the molar gas constant and equilibrium pressure, p (Pa).

At low adsorbate loading (~0.002–0.03 mg mg^{-1}), Q_{st} for the fresh PtH-MFI-15 catalyst was found to be ~27–29 kJ mol^{-1}. For samples following increasing TOS, the low loading (~0.004–0.03 mg mg^{-1}) Q_{st} increased to ~32–34 kJ mol^{-1} for the 4 h and 24 h coked PtH-MFI-15 catalysts. For the 48-h coked PtH-MFI-15 sample, Q_{st} increased from a value of ~18 kJ mol^{-1} at very low loading (<~0.004 mg mg^{-1}) to a maximum value of 23.5 kJ mol^{-1} at 50% of the maximum uptake of eight molecules *per* unit cell. A further increase in the ethane loading for this sample led to a decrease in the Q_{st} due to the balance between the two opposing interactions (surface attraction and intermolecular repulsion) of the ethane molecules. The behaviour of the sample obtained after 48 h TOS is associated with a significant decrease in the total accessible volume available for a given adsorbate loading by this time.

4.8. Mass transfer coefficient

Kinetics data from ethane adsorption experiments were used to determine the variation of the mass transfer coefficients (MTC) with adsorbate uptake. Since the kinetics data were obtained in the course of obtaining an equilibrium adsorption isotherm, the pressure step sizes employed were small. The upper regions ($M(t)/M(\infty) > 0.5$) of each of the experimental kinetic uptake curves were fitted to an equation of the same mathematical form as the linear driving force (LDF) model [17]:

$$\frac{M(t)}{M(\infty)} = 1 - \exp(-kt) \tag{8}$$

where $M(t)$ is ethane uptake at time t (normalised so that $M(0) = 0$), $M(\infty)$ is the equilibrium uptake and k is the mass transfer coefficient (MTC). Glueckauf [18] has shown that, for the upper region of the uptake curve approaching equilibrium, the series solution of the diffusion equation for spherical geometry with a step change in external pressure reduces to the same mathematical form as the LDF model. Hence, for intra-crystalline diffusional control, the MTC, k, is equivalent to $15D/a^2$ [17], where D is the internal effective diffusivity and a is the effective (crystallite) spherical radius (diffusion length). The MTC was subsequently corrected for the slope of the equilibrium adsorption isotherm of ethane at the same coverage, as suggested by Crank [19].

Fig. 13 shows the change of the MTC with TOS, obtained from fitting the LDF model. It can be seen that, at a constant amount of ethane adsorbed, an increase in the MTC was observed with TOS for the PtH-MFI-15 catalyst. However, coke deposition up to 2 mass % did not affect diffusion of ethane in the PtH-MFI-40 catalyst. The MTC for the coked PtH-MFI-40 catalysts was the same as that in the fresh catalyst. After 48 h on-stream, the PtH-MFI-15 catalyst yielded a larger MTC when compared to the PtH-MFI-40 catalyst, at a specific amount of ethane adsorbed.

While several workers [20,21] have shown that surface diffusion barriers do not exist for many systems, barrier effects at the surface of zeolite crystallites may sometimes control mass uptake rates in kinetic experiments [22]. The influence of the surface barrier is dependent on the surface area to volume ratio of the crystallites. Further, Chen et al. [23] suggest that the barrier should increase in influence when the crystallite size decreases, since the number of pore openings would then increase sharply. Hence, previous work suggests that if uptake rate is controlled by the surface barrier effect, then it should be sensitive to the (apparent) surface area to volume ratio of the crystallites and/or the number of pore openings in the exterior of the crystallites. As shown in Table 2, the results of the two-component model fit to the gas adsorption data for the PtH-MFI-40 catalyst suggest that the external surface area of the zeolite crystallites, as measured by the BET surface area, is changed significantly by coking. This would suggest that the apparent surface area of the zeolite crystallites is changed for this sample, and there-

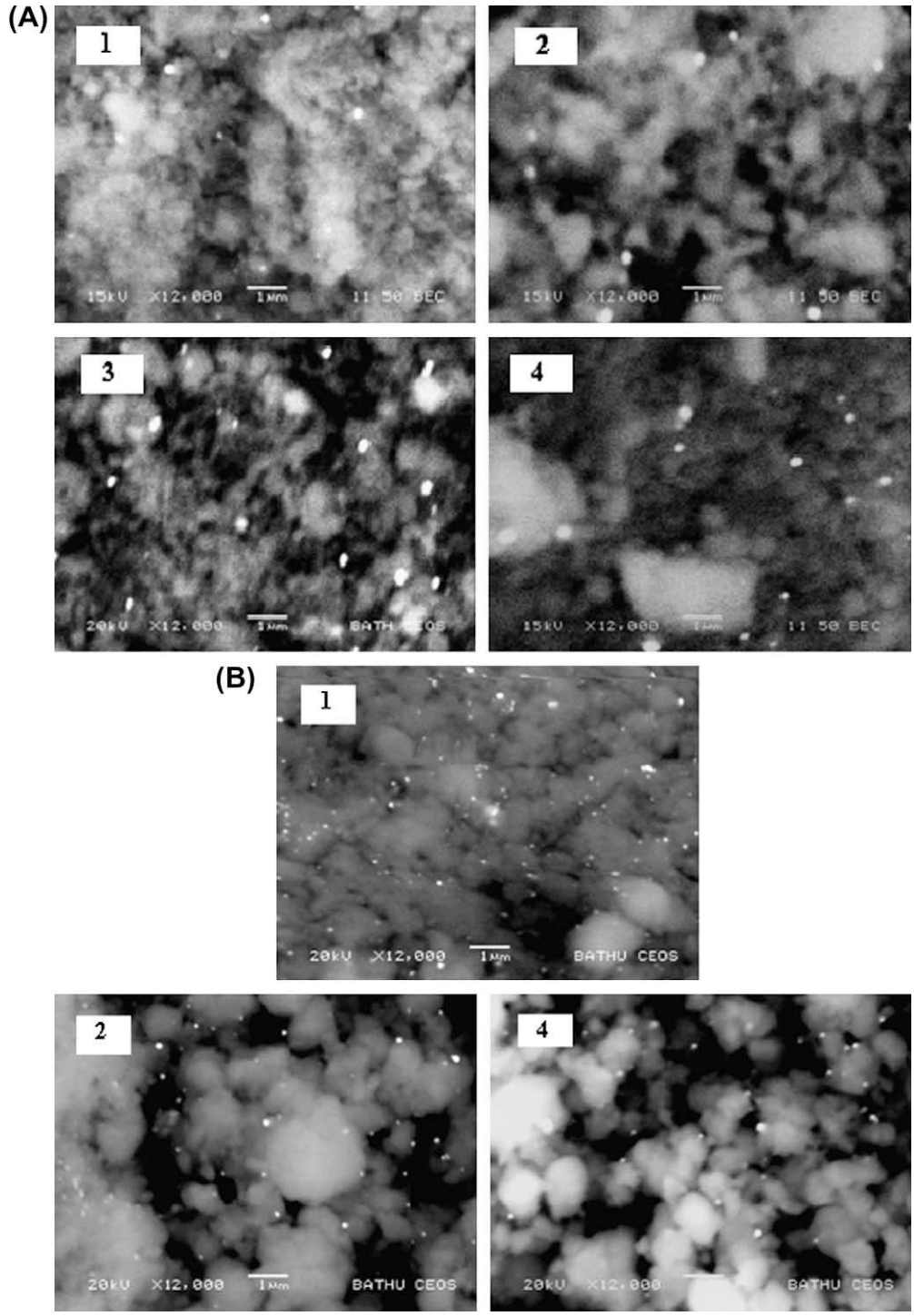

Fig. 12. Backscattered scanning electron microscopy images of PtH-MFI-15 (A) and PtH-MFI-40 (B) catalysts: fresh (1), 4 h (2), 24 h (3) and 48 h (4) on-stream.

Table 3
Effect of time-on-stream (TOS) on the concentration of platinum particles on the surface of the PtH-MFI-15 and PtH-MFI-40 crystallites.

Time-on-stream (h)	Concentration (number of Pt particles *per* μm^2)	
	PtH-MFI-15	PtH-MFI-40
0	0.134 ± 0.003	0.520 ± 0.033
4	0.129 ± 0.008	0.204 ± 0.045
24	0.142 ± 0.014	–
48	0.135 ± 0.014	0.131 ± 0.013

fore the progressive coke laydown for this material ought to lead to a change in the size of the surface barrier effect, by, for example, changing the number of accessible pore openings. If this surface barrier was the rate-limiting mass transport process, then this change also ought to be apparent in the observed mass transport rate. However, coking of the PtH-MFI-40 catalyst does not lead to a significant change in mass transport rates and thus we can conclude that the surface barrier is not the rate-limiting step. Since the laydown of coke within the mesopores of the

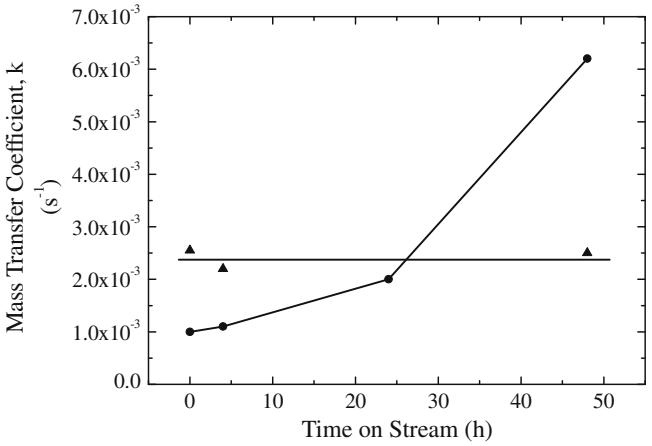

Fig. 13. MTC variation with time-on-stream (TOS) for PtH-MFI-15 (●) and PtH-MFI-40 (▲) catalysts at ethane loading of 6 molecules *per* unit cell. (The lines shown are to guide the eye.)

PtH-MFI-40 catalyst also ought to be expected to affect mesopore mass transport rates, the lack of a change in observed mass transport rate for this material also suggests that mesopore mass transport rates cannot be the rate-limiting step.

The diffusion of molecules on surfaces can be considered as a series of activated hops between adsorption sites. If the diffusion is modelled as a random walk, then diffusivity, D is given by:

$$D = \frac{k_D \lambda^2}{\tau} \tag{9}$$

where λ is the jump distance, τ is the correlation time and k_D is a numerical factor which depends on the dimensionality of the system. If the diffusion of molecules is an activated process, in which the diffusivity varies with temperature, the diffusivity may be correlated with an Arrhenius expression of the form of:

$$D = D_o \exp\left(\frac{E_D}{RT}\right) \tag{10}$$

where D_o is the pre-exponential factor and E_D is the activation energy for diffusion.

Since the activation energy for the correlation time is a monotonically increasing function of the differential, isosteric enthalpy of adsorption, Q_{st} [24], the correlation time for diffusion should increase with 0–24 h TOS for the PtH-MFI-15 catalyst, as the strength of the interaction, between ethane molecules and the pore walls, increases. This is supported by the increase in Q_{st} for the coked PtH-MFI-15 catalysts as described in Section 4.7. As a result of site blockage, or increasing adsorption coverage, the jump length of the molecule is reduced due to intermolecular collisions. Hence, the contributions from both the jump length and the correlation time suggest that the diffusivity of the ethane molecules should decrease with TOS.

Since the diffusivity of ethane did not increase with coking, then the observation of an increase in MTC ($k = 15D/a^2$) with coking (Fig. 13) for the PtH-MFI-15 catalyst can only be explained by a decrease in the length of the diffusion pathway, which is equivalent to an apparent decrease in the crystallite size of the zeolite catalyst. The decrease in the diffusion path length but lack of impact on diffusivity can be explained by the preferential deposition of coke towards the centre of the zeolite crystallites, thereby partially blocking the internal pore structure of the PtH-MFI-15 zeolite catalysts [6,25].

5. Discussion

5.1. Activity and selectivity of the PtH-MFI zeolites

During the alkylation reaction of benzene with ethane, both PtH-MFI catalysts yielded ethane conversions higher than the expected equilibrium conversion of ethane from dehydrogenation (~0.55%) [3,4]. The PtH-MFI-15 catalyst yielded a larger ethane conversion, but lower stability of the catalyst as illustrated by the drop in the conversion of the reactants with time. With the greater number of acid sites associated with the PtH-MFI-15 catalyst, the alkylation reaction of benzene with ethene was enhanced, hence drawing the ethane dehydrogenation reaction forward. As a result, the selectivity to ethene for the PtH-MFI-15 catalyst is lower than that observed for the PtH-MFI-40 catalyst.

As with the conversion of ethane, benzene conversion to EB alone would also be limited by thermodynamics, and the equilibrium conversion of benzene into EB was calculated to be 13.5% [3,4]. However, the conversion of benzene over the PtH-MFI-15 catalyst exceeded this equilibrium conversion and gave a benzene conversion of 20.5% at the start of the reaction. This suggests that benzene was also converted into other products as well as the transformation of benzene into EB.

From Fig. 3, it follows that the selectivity of the desired product, EB was increasing with TOS. The gain in EB selectivity could be associated with the decrease in selectivity to toluene, xylene, triethylbenzene and ethyltoluene. Due to the higher number of acid sites for the PtH-MFI-15 catalyst, the EB selectivity is lower, when compared with the corresponding selectivities observed with the PtH-MFI-40 catalyst, because, subsequent to its initial formation, EB was then more likely to be transformed into other aromatic products on the additional acid sites.

The variations in the shape-selective reactions that take place during the alkylation reaction of benzene with ethane, such as the alkylation of EB with ethene to form DEB and the EB hydroisomerization reaction to produce xylenes, over the PtH-MFI-15 catalyst showed the effect of catalyst deactivation as opposed to the stable performance of PtH-MFI-40 catalyst. Further explanation for this observation will be given in later sections.

5.2. Pore structure modification

The modification of the pore architecture of the PtH-MFI catalysts with TOS was observed from the nitrogen and argon adsorption results. The difference between the total nitrogen and argon adsorption capacity of the fresh and deactivated catalysts is believed to be associated with the increasing coke content with higher TOS. The isotherm shift observed (Figs. 7 and 8) for the coked catalysts could possibly be due to the effect of coke deposition during the alkylation reaction.

From the adsorption isotherm data, the pore size distribution (PSD) of the PtH-MFI catalysts was obtained using the Horvath–Kawazoe cylindrical pore model for the nitrogen adsorption data (Fig. 14). It should be noted that due to the simple description of the adsorbate–adsorbent interactions in the HK model, the PSD generated from it probably does not give a correct absolute pore size for the MFI catalyst. Hence, only the relative shift in the PSD is taken into account, which may reflect geometric or chemical changes, or both together. The differential pore volume plot of the fresh catalyst showed three peaks at 0.725 nm, 0.743 nm and 0.749 nm. As the carbon content increased, the intensity of the three peaks progressively decreased, and the PSD was shifted towards smaller pore diameters. A significant apparent increase in the micropore volume was observed at a pore diameter of 0.72 nm for the 4 h coked catalyst and 0.71 nm for the 24 h coked

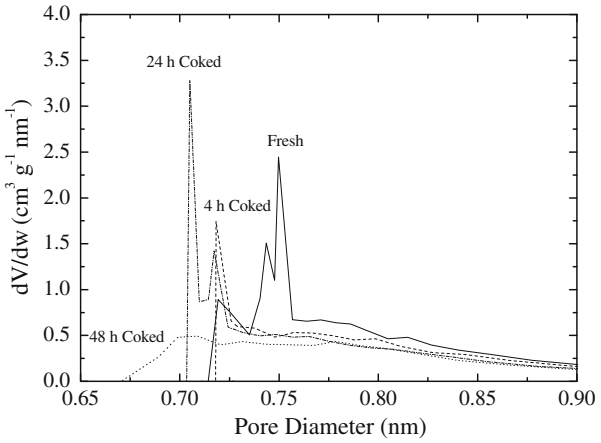

Fig. 14. Pore size distribution for the PtH-MFI-15 catalyst obtained from the N_2 (at 77 K) isotherms using the Horvath–Kawazoe method: fresh (solid line), coked samples after 4 h (dashed line), 24 h (dash-dot-dot line) and 48 h (dotted line) time-on-stream (TOS).

catalyst. In the case of the PtH-MFI-15 catalyst coked for 4 and 24 h, the modification of the micropore size distribution could result from coke deposition onto the walls of larger micropores, hence apparently creating more smaller pores. A general trend towards apparently smaller pores with increased TOS might also arise from the increasing formation of more dead-end pores as coke is deposited within the core of the crystallites. This is because adsorption occurs more readily (at lower pressure) in dead-end pores due to the increased pore potential.

5.3. Coke location

The identification of the particular location of coke deposits is important to understanding the mechanism of coking during the benzene alkylation reaction. Changes in the relative position and intensities of XRD peaks have previously been suggested to result from the distortion of the MFI lattice when it was occluded by template ions [5] or when carbonaceous materials were deposited within the zeolite pores [12]. The similar changes, observed in this work, when comparing the XRD spectra of the fresh and coked PtH-MFI-15 catalyst to those reported in the recent study by Lin et al. [12] provide evidence that the deposited coke was located inside the zeolite channels as opposed to the external location of the coke formed during the alkylation reaction over the PtH-MFI-40 catalyst.

The change in the ratios of the adsorption capacity parameters, from the two-component (Langmuir and BET) adsorption fits, with TOS suggested that that the deposition of coke within the PtH-MFI-40 catalyst was dominated by pore blockage, where the entrance to the zeolite channels was blocked by coke forming on the outside of the zeolite crystallite. However, a different mechanism was proposed for the higher activity catalyst with the greater number of acid sites (PtH-MFI-15), since only the Langmuir component adsorption capacity was changing with TOS, and no significant variation was observed for the BET component adsorption capacity. Hence, only the pores within the zeolite crystallites were modified by coke, supporting the location of coke deposition suggested by the XRD spectra.

If the coke were blocking access to pores which did not contain coke molecules, then the difference between the accessibility fraction and the fraction of unplugged pores (Fig. 9) would have been significant. In the case of pore mouth plugging, a small amount of coke on the surface of the zeolite crystallite can lead to a large decrease in the accessibility of the molecules to the centre of the catalyst. In addition, if the percolation threshold (f_c) of the lattice was reached, the pore network would lose its connectivity, resulting in the complete loss in accessibility. However, this was not observed in our results for the PtH-MFI-15 catalysts even when the percolation threshold for the lattice, assuming a random distribution of coke, was reached. Fig. 9 shows that the PtH-MFI-15 pore network remained highly accessible to nitrogen and argon even when the percolation threshold for random deposition was reached. The bond-site percolation threshold ($f_c = 0.64$) value was evaluated from blocking the bonds and sites randomly with coke molecules. Two different gases with different potential interactions with the surface were used. Nitrogen has a permanent quadrupole moment, while argon is a spherically symmetric (though polarisable) molecule. Since both gases gave similar results, this suggests that accessibility was not affected by chemistry.

A comparison of the accessibility plots (Fig. 9), for the homogeneous laydown model and the experimental results, suggested that all remaining vacant sites, following coking, belong to the percolating cluster for the real system. This finding suggests the spatially correlated laydown of coke due to it growing preferentially on existing coke species for the following reasons. The shape of the experimental accessibility function suggests two potential scenarios. First, the laydown of coke as part of, potentially spatially extended, but isolated, islands throughout a zeolite crystallite would be consistent with the gas adsorption accessibility data if the remaining free pore space remained connected with the surface. However, the islands of coke would act as barriers to diffusion and thus increase tortuosity because the incoming diffusion flux is forced to deviate around them. Hence, diffusivity, and thus the MTC, would then be expected to decrease with increasing TOS and coke levels for the PtH-MFI-15 catalyst. However, the opposite is observed and thus this scenario must be incorrect. The second spatially correlated scenario is where coke molecules are initially formed in the core of a crystallite (or fused cluster of crystallites), and as the coke content increased, these coke molecules block the channels and intersections in such a way that the coke was progressively building up from the middle of the structure, moving outwards towards the crystallite surface, hence only decreasing the diffusion length of the zeolite crystallites, and thereby increasing the MTC.

5.4. The deactivation behaviour of the PtH-MFI catalyst

In order to determine whether the shape-selectivity of the PtH-MFI catalyst was enhanced or decreased by coke deposition, the product selectivity of the DEB and xylene isomers was analyzed. It was pointed out earlier that the selectivity to *para*-DEB was decreased, while the selectivity to *meta*-DEB was increased, with TOS for the reaction carried out over PtH-MFI-15 catalyst. Due to the steric constraints of the two ethyl groups, *ortho*-DEB was not observed in the product distribution. This finding is rare in comparison with the typical effect of coking, which would enhance the selectivity of *para*- isomers as the effective channel size of the catalyst is reduced, and the diffusion resistance increased, with coke deposition [12].

It was previously [26] suggested that an increase in the crystallite size of ZSM-5 would increase its diffusion path length leading to increased selectivity of *para*-isomers because the DEB isomers would then have to travel a long distance before they left the crystallites. In this work, however, the selectivity of *meta*-DEB was increased with TOS as the *meta*-DEB did not isomerize to form *para*-DEB (Eq. (11)). This could possibly be the effect of coke decreasing the diffusion pathway as evaluated from the variation in the MTC results (Section 4.8).

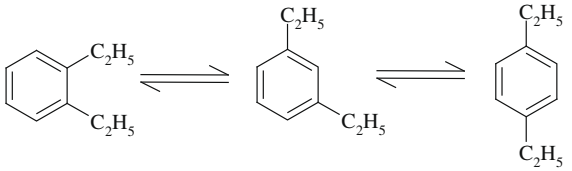

(11)

As for the variation of the xylene isomers distribution with TOS, the deactivated catalysts, which have smaller diffusion length, are always less *para*-selective than the fresh Pt-modified MFI-15 catalyst (Fig. 5). The relationship between the xylene isomers selectivity with TOS shows that the *ortho*-xylene selectivity was increasing at the expense of the *meta*- + *para*-xylene selectivity. This result was consistent with previous research on toluene alkylation with methanol by Sotelo et al. [6], who suggested that pore blockage by coke molecules leads to a decrease in the diffusion pathway length, thus decreasing the *para*-selectivity of the xylene isomers.

As opposed to the effect of coke seen on the PtH-MFI-15 catalyst, the coking phenomenon had no effect on the shape-selectivity reactions when the reaction was carried out with the PtH-MFI-40 catalyst. In the discussion earlier, it was proposed that the deposition of coke within the zeolite crystallites and the reduction in the diffusion length of the PtH-MFI-15 catalyst were responsible for the changes in the selectivity of different isomers with TOS. With coke deposition on the external surface of the zeolite crystallites, as shown by the diffraction spectra and adsorption results for the PtH-MFI-40 catalyst, no variations in the DEB isomers with TOS was observed. In addition, the diffusion path length of the PtH-MFI-40 catalyst remained long with TOS when compared to the PtH-MFI-15 catalyst, as demonstrated by the larger MTC for the PtH-MFI-15 catalyst. The differences between the two observations emphasised the different effects/modes of coke formation, mainly depending on the location of coke. The cause of the spatial variation in coke observed for the two PtH-MFI catalysts of different Si/Al ratio is being investigated and will be the subject of discussion in future publications.

6. Conclusions

This work has demonstrated the different coking behaviour of the bifunctional PtH-MFI-15 and PtH-MFI-40 catalysts during benzene alkylation with ethane at 370 °C. During the alkylation reaction of benzene with ethane over the PtH-MFI-15 catalyst, the conversion of benzene and ethane decreased with TOS as a result of catalyst deactivation. On the other hand, the PtH-MFI-40 catalyst remained stable during the alkylation reaction even with increasing coke content as determined by thermogravimetric analysis.

The XRD patterns, together with the sorption data for the different probe molecules, suggest that coke is deposited inside the pores of the zeolite catalysts for the PtH-MFI-15 catalyst, while coke is mainly formed on the outside of the zeolite crystallites when the alkylation reaction is carried out over the PtH-MFI-40 catalyst. It was proposed from the accessibility function derived from nitrogen and argon sorption data that, with prolonged TOS, the coke molecules build up from the middle of the zeolite crystallites outwards towards the surface of the crystal, as the reaction was carried out over the PtH-MFI-15 catalyst. As a result, the diffusion length of the PtH-MFI-15 crystallites decreased with TOS, confirming the interpretation made of the mass transfer coefficient variation with TOS obtained from the ethane adsorption experiments.

The decreasing diffusion path length of the PtH-MFI-15 catalyst increased the selectivity towards *meta*-DEB and *ortho*-xylene at the expense of *para*-DEB and *meta*- + *para*-xylene selectivity, respectively. In contrast, for the PtH-MFI-40 catalysts, no variations in the DEB isomers were observed.

Acknowledgment

The authors thank EPSRC for financial support (under Grant No. EP/C532554).

References

[1] T.F. Degnan, C.M. Smith, C.R. Venkat, Applied Catalysis. A, General 221 (2001) 283–294.
[2] J.A. Moulijn, M. Makkee, A. van Diepen, Chemical Process Technology, John Wiley & Sons, Ltd., pp. 109–130.
[3] D.B. Lukyanov, T. Vazhnova, Journal of Molecular Catalysis A: Chemical 279 (2008) 128–132.
[4] D.B. Lukyanov, T. Vazhnova, Journal of Catalysis 257 (2008) 382–389.
[5] D.M. Bibby, N.B. Milestone, J.E. Patterson, L.P. Aldridge, Journal of Catalysis 97 (1986) 493–502.
[6] J.L. Sotelo, M.A. Uguina, J.L. Valverde, D.P. Serrano, Applied Catalysis A: General 114 (1994) 273–285.
[7] A. De Lucas, P. Canizares, A. Durfin, A. Carrero, Applied Catalysis A: General 156 (1997) 299–317.
[8] M. Guisnet, P. Magnoux, Applied Catalysis 54 (1989) 1–27.
[9] M.A. Uguina, D.P. Serrano, R. Van Grieken, S. Venes, Applied Catalysis A: General 99 (1993) 97–113.
[10] D.H. Olson, W.O. Haag, ACS Symposium Series 248 (1984) 275–307.
[11] W.H. Chen, T.C. Tsai, S.J. Jong, Q. Zhao, C.T. Tsai, I. Wang, H.K. Lee, S.B. Liu, Journal of Molecular Catalysis A: Chemical 181 (2002) 41–55.
[12] X. Lin, Y. Fan, G. Shi, H. Liu, X. Bao, Energy and Fuels 21 (2007) 2517–2524.
[13] B.L. Trout, A.K. Chakraborty, A.T. Bell, Chemical Engineering Science 52 (1997) 2265–2276.
[14] F. Moreau, N.S. Gnep, S. Lacombe, E. Merlen, M. Guisnet, Applied Catalysis: A General 230 (2002) 253–262.
[15] R.E. Richards, L.V.C. Rees, Langmuir 3 (1987) 335–340.
[16] C.A. Fyfe, G.J. Kennedy, C.T. De Shutter, G.T. Kokotailo, Journal of Chemical Society-Chemical Communication (1984) 541–542.
[17] S. Sircar, J.R. Hufton, Adsorption 6 (2000) 137–147.
[18] E. Glueckauf, Transactions of the Faraday Society 51 (1955) 1540–1551.
[19] J. Crank, The Mathematics of Diffusion, Clarendon Press, Oxford, 1975.
[20] J. Kärger, D.M. Ruthven, Zeolites 9 (1989) 267–281.
[21] J. Kärger, H. Pfeiffer, J. Caro, M. Bülow, H. Schloder, R. Mostowicz, J. Völter, Applied Catalysis 29 (1987) 21–30.
[22] M. Bülow, P. Struve, G. Finger, C. Redszus, K. Ehrhardt, W. Schirmer, J. Kärger, Journal of the Chemical Society Faraday Transactions I 76 (1980) 597–615.
[23] D. Chen, H.P. Rebo, A. Holmen, Chemical Engineering Science 54 (1999) 3465–3473.
[24] E.R. Gilliland, R.F. Baddour, G.P. Perkinson, K.J. Sladek, Industrial & Engineering Chemistry Research 13 (1974) 95–100.
[25] D. Chen, H.P. Rebo, K. Moljord, A. Holmen, Chemical Engineering Science 51 (1996) 2687–2692.
[26] N.Y. Chen, W.W. Kaeding, F.G. Dwyer, Journal of American Chemical Society 101 (1979) 6783–6784.